1

A Field Study of Pixel-Scale Variability of Raindrop Size Distribution in the

2

Mid-Atlantic Region

3

4

*Ali Tokay**

5

Joint Center For Earth Systems Technology, University of Maryland Baltimore County

6

and NASA Goddard Space Flight Center, Greenbelt, Maryland

7

Leo Pio D'Adderio

8

Department of Physics and Earth Science, The University of Ferrara, Ferrara, Italy

9

David B. Wolff and Walter A. Petersen

10

NASA Goddard Space Flight Center, Wallops Flight Facility, Wallops Island, Virginia

11

12

15

16

17

18

* Corresponding author's address:

19

NASA Goddard Space Flight Center, Code 612.0

20

Greenbelt, MD 20771

21

tokay@umbc.edu

22

23

24   Abstract

25

26   The spatial variability of parameters of raindrop size distribution and its derivatives

27   is investigated through a field study where collocated PARSIVEL[2] and two-

28   dimensional video disdrometers are operated at six sites in Wallops Island, Virginia

29   from December 2013 to March 2014. The three-parameter exponential function is

30   employed to determine the spatial variability across the study domain where the

31   maximum separation distance was 2.3 km. The nugget parameter of exponential

32   function is set to 0.99 and the correlation distance (d_0) and shape parameter (s_0) are

33   retrieved minimizing root-mean-square error, after fitting it to the correlations of

34   physical parameters. Fits were very good for almost all fifteen physical parameters.

35   The retrieved d_0 and s_0 were about 4.5 km and 1.1, respectively, for rain rate (RR)

36   when all twelve disdrometers were reporting rainfall with a rain rate threshold of

37   0.1 mm h^{-1} in one-minute observations. The d_0 decreased noticeably when one or

38   more disdrometers were required to report rain. The d_0 was considerably different

39   for a number of parameters (e.g. mass weighted diameter) but was about the same

40   for the other parameters (e.g. RR) when rainfall threshold was reset to 12 dB for Ka-

41   band and 18 dB for Ku-band reflectivity following the expected Global Precipitation

42   Measurement mission's space-borne radar minimum detectable signals.   The

43   reduction of the database through elimination of a site did not alter d_0 as long as the

44   fit was adequate. The correlations of 5-minute rain accumulations were lower when

45   disdrometer observations were simulated for a rain gauge at different bucket sizes.

46

47   1. Introduction

48

49   The National Aeronautics and Space Administration (NASA) Global Precipitation

50   Measurement (GPM) mission aims to retrieve the three dimensional hydrometeor

51   size distribution of precipitation through its Dual-frequency Precipitation Radar

52   (DPR) on board the GPM core satellite (Hou et. al. 2014). The retrieval algorithm

53   outputs parameters of gamma model size distribution for each range bin utilizing

54   Ka- and Ku-band radar measurements (Seto et al. 2013). The lowest clutter free

55   range bin near the surface at nadir incidence is approximately 5 km radius and 125

56   m height. One of the key uncertainties of retrieved size distributions is its spatial

57   variability within a given DPR footprint.   The spatial variability is a result of

58   precipitation gradient within the range volume, which may not be completely

59   covered by the precipitation. This variability contributes to Non-Uniform Beam

60   Filling (NUBF) which results in a higher degree of uncertainty in microwave sensor

61   based precipitation estimates where the instantaneous field of view is typically

62   bigger than the DPR footprint (Tokay et al. 2014a).

63

64   Scanning radars in range height indicator mode provides the most relevant data

65   source to study the spatial variability of hydrometeor size distribution in the

66   vertical, while gridded radar data at 1x1 km or 2x2 km resolution is a common

67   resource for studying the horizontal spatial variability.   The parameters of the size

68   distribution that are derived from radar measurements are based on empirical

69   relationships (Bringi et al. 2004). There is also an uncertainty within the radar pixel

70   as its size increases away from radar. Disdrometers are an alternative resource for

71   estimating the horizontal spatial variability but are associated with point sampling

72   and it is quite costly to populate a dense network with disdrometers to sample the

73   area of a satellite footprint. Therefore, there have been relatively few field studies

74   conducted to determine the spatial variability of hydrometeor size distributions and

75   all of these dealt with rainfall.

76

77   As part of the NASA's Tropical Rainfall Measurement Mission (TRMM) Ground

78   Validation program, a number of impact type Joss-Waldvogel disdrometers were

79   first deployed during a series of field campaigns and also deployed later at the NASA

80   Wallops Flight Facility on Wallops Island, Virginia. The latter operation allowed for

81   determination of the measurement accuracy of the disdrometers when six units

82   were side-by-side (Tokay et al. 2005) and the spatial variability of raindrop size

83   distribution (DSD) when three units were deployed across the Wallops Island strip,

84   where the minimum and maximum separation distances were 0.65 and 1.7 km,

85   respectively (Tokay and Bashor 2010). Later, four disdrometers were distributed

86   across the same strip where the minimum and maximum separation distances were

87   0.4 and 5.0 km, respectively (Schröer 2011). The three-parameter exponential

88   function was tested to determine the spatial variability of DSD and integral rain

89   parameters. Since four disdrometers provide six pairs of correlations across 5 km,

90   the fitted exponential function was subject to noticeable error.

91

4

92   Measurement accuracy is one of the key uncertainties in determining the spatial

93   variability of DSDs quantitatively. Each disdrometer type has its own shortcomings

94   in measuring the DSD, and comparative field studies where different types of

95   disdrometers were collocated, help quantify the uncertainties of the disdrometers

96   (Krajewski et al. 2006, Thurai et al. 2011, Tokay et al. 2013, 2014b). Indeed, the

97   Miriovsky et al. (2004) pioneer study was unable to determine the spatial variability

98   of reflectivity within 1 km^2 due to uncertainties of four different types of

99   disdrometers. Lee et al. (2009), on the other hand, used four Particle Occurrence

100 Sensor System (POSS) to study the spatial variability of DSD in stratiform rain

101 events. An S-band dual polarization radar scanned over the POSS units and the

102 spatial correlation of rainfall was higher in radar than in POSS especially at 15 and

103 30 km. This could partly be due to the differences between the sampling volumes of

104 the instruments.

105

106 The first comprehensive field study to quantify the spatial variability of the DSD was

107 conducted in Central Spain where eight dual PARSIVEL (PARticle Size VELocity)

108 disdrometers were deployed (Tapiador et al. 2010). The availability of number of

109 disdrometers allowed 28 pairs of correlations where the distances range from 0.2

110 km to 3.2 km.   The dual units were aligned in both North-South and East-West

111 directions, and one of the five events had significant differences in correlations of

112 reflectivity between North-South and East-West aligned disdrometers. Jaffrain et al.

113 (2011), on the other hand, analyzed 53 hours of 16 PARSIVEL observations to

114 determine the spatial variability of DSD in a radar pixel (about 1 x 1 km^2) in

115   Lausanne, Switzerland. They concluded that the coefficient of variations for the

116   mass weighted diameter (D_{mass}), total concentration (N_T), and rain rate (RR) were

117   high and could not be explained solely by the uncertainty of the measurement.

118   Jaffrain and Berne (2012, JB12 hereafter) used the same set up of instruments to

119   determine the spatial variability of D_{mass}, N_T, and RR using a variogram analysis.

120   They reported that the variability was greater in convective rain than transitional

121   and frontal rain. They also noted a decreasing variability with decreasing temporal

122   resolution. Perhaps, the main issue of these studies is the measurement accuracy of

123   the PARSIVEL disdrometer. The low-cost laser resulted in overestimation of large

124   drops due to an inhomogeneous beam (Thurai et al. 2011, Tokay et al. 2013). The

125   manufacturer upgraded the PARSIVEL disdrometer with PARSIVEL[2] in 2011 (Tokay

126   et al. 2014b).

127

128   In contrast to disdrometers, rain gauges are low-cost, durable, easy to maintain and

129   are frequently deployed to adjust or validate radar rainfall estimates during either

130   two-month long field studies or longer-term field observations. Thus, rain gauge

131   networks are an excellent resource to study the spatial variability of rainfall (Habib

132   and Krajewski 2002, Gebremichael and Krajewski 2004, Ciach and Krajewski 2006,

133   among others). The spatial variability of rainfall is often quantified applying a three-

134   parameter exponential function to the corrections between the paired gauge

135   measurements. The parameters of the exponential function differs from one study

136   to another due to the differences in quality of rain gauge data, inter-gauge distances,

137   sample size, experiment period and location (Villarini et al. 2008). Logistics may

138   limit the inter-gauge distances, while long-term observations with dual or multiple

139   gauge at each site has a clear advantage for a larger sample size and continuous

140   gauge record at a given gauge site. The long-term observations also allow

141   investigation of season-to-season differences in the spatial variability of rainfall.

142   Tokay et al. (2014a), for instance, used five years of continuous rain gauge

143   measurements in the Southern Delmarva Peninsula and showed that weather

144   systems dominate spatial variability over a season. Nor'easters, for instance,

145   dominate winter precipitation in the Mid-Atlantic region.

146

147   As a comparative study, the spatial variability of rainfall was quantified through X-

148   band radar and rain gauge network (Moreau et al. 2009). The correlations between

149   the paired radar pixels at 1 km^2 resolution were significantly higher than those

150   between paired gauges underneath the radar pixel up to 8 km. The differences in

151   correlations are attributed to the differences in sampling volume, while the errors in

152   radar rainfall estimate and time-height ambiguity also be played a role. Another

153   comparative study of the spatial variability of rainfall was conducted using S-band

154   dual-polarization radar and 2DVD measurements during Mid-latitude Continental

155   Convective Clouds Experiment (MC3E) (Bringi et al. 2015). A good agreement was

156   found between the radar and disdrometer based spatial variability for RR, median

157   volume diameter, and logarithmic normalized intercept parameter with respect to

158   liquid water content (N_W) in a long lasting stratiform event. The correlation

159   distances were lower in a relatively short convective event than the stratiform event

160   for all three parameters.

161

162   This study investigates the pixel-space variability of DSD and integral rain

163   parameters employing a disdrometer network at NASA Wallops Flight Facility

164   (WFF), Wallops Island, Virginia (37.9 degree N and 75.4 degree W). The manuscript

165   is organized as follows: The disdrometer network and the database are presented in

166   Section 2. Section 3 introduces the three-parameter exponential function while the

167   parametric form of the DSD is given in Section 4. The probability and cumulative

168   distributions of the DSD and rain parameters can be found in Section 5. Section 6

169   depicts the spatial variability of DSD and rain parameters, while the sensitivity

170   studies are in Section 7. The conclusions are given in the last section.

171

172   2. Field Study

173

174   The disdrometer network consists of six sites where each site had one two

175   dimensional video disdrometer (2DVD) and one PARSIVEL[2] disdrometer. The sites

176   were distributed across WFF where the minimum and maximum separation

177   distances were 0.5 and 2.3 km, respectively (Figure 1a). One of the sites (Pad)

178   hosted a variety of tipping and weighing bucket rain gauges including two pit gauges

179   (Figure 1b). Another site was collocated with the Wallops Automated Surface

180   Observing System (ASOS) as well as additional tipping bucket rain gauges (Figure

181   1c). Table 1 summarizes the locations and distances between the sites.

182

183 PARSIVEL[2] is the third generation of the laser-optical PARSIVEL disdrometer

184 (Tokay et al. 2014b). It is designed to measure the size and fall velocity of individual

185 hydrometeors across its laser beam and is also present weather sensor. For rain,

186 PARSIVEL outputs drop counts in a 32 x 32 size versus fall velocity matrix at

187 selected time intervals ranging from 10-second to one-minute. The first two size

188 bins are empty due to low signal to noise ratio and the smallest measurable

189 raindrop corresponds to 0.25 mm diameter. The width of the size bins increases

190 with the size of raindrops from 0.125 mm for drops to 1.2 mm, to 0.25 for drops up

191 to 2.5 mm, to 0.5 mm for drops up to 5 mm, and to 1.0 mm for the larger drops.

192 Therefore, there is noticeable uncertainty in determining the maximum drop size of

193 the DSD. Based on 2DVD observations, the largest raindrop ever recorded is 9.7 mm

194 diameter (Gatlin et al. 2015). The 25th bin corresponds to 9-10 mm and was

195 considered as the largest bin for rain. For fall velocity, PARSIVEL has a range from

196 0.05 to 20.8 m s^{-1}, covering fall speeds of all types of hydrometeors. For rain, the

197 26th bin corresponds to 8-9.6 m s^{-1}, and covers the expected range for terminal fall

198 speeds of very large raindrops (Beard 1976). However, PARSIVEL[2] underestimates

199 the fall velocity of raindrops by approximately 1 m s^{-1} with respect to the expected

200 terminal fall speed of raindrops at around 1 mm diameter (Tokay et al. 2014b). The

201 underestimation in fall velocity is also evident for larger drops but the difference

202 between the mean PARSIVEL[2] and terminal fall speed decreases with increasing size.

203 The manufacturer recognizes this matter as a software error and it is expected that

204 the new generation of instruments will mitigate this issue (Kurt Nemeth, OTT

205 PARSIVEL, *personal communication*, 2015).

206

207 The 2DVDs are the "compact" third generation and are composing of sensor unit and

208 indoor personal computer (Schönhuber et al. 2007). The third generation compact

209 version has the optical components firmly mounted with no need for re-alignment

210 by the user. The distance of the optical slits to the rim of the housing was also

211 reduced aiming to eliminate inhomogeneous filling of the measurement area in

212 windy conditions. The high-speed line-scan cameras provides better matching of

213 falling hydrometeors between the two planes that are nominally 6 mm apart. The

214 2DVD records the time stamp of each raindrop including its equivalent diameter, fall

215 velocity, and oblateness as well as the sampling area. Common interruption of data

216 occurs often due to non-meteorological items (e.g. leaves) in the sampling cross

217 section, which is the main shortcoming of the 2DVD.

218

219 The dataset for this study spanned from December 2013 through March 2014.

220 While PARSIVEL[2] disdrometers operated nearly continuous during the experiment

221 period, a number of 2DVD units failed to operate in a few rain events. The raw

222 outputs of PARSIVEL[2] and 2DVD observations were integrated to one-minute after

223 screening secondary and mismatched drops that fell outside ±50% of their terminal

224 fall speed (Tokay et al. 2013). Several rain/no-rain thresholds were then applied to

225 the one-minute observations. All thresholds required a minimum of 10 drops. The

226 minimum RR of 0.1 mm h^{-1} resulted in 447 one-minute samples when all twelve

227 disdrometers reported rainfall. Considering the minimum detectable reflectivity of

228 the GPM DPR, the Ku-band reflectivity (Z_{Ku}) of 18 dB and Ka-band reflectivity (Z_{Ka})

229   of 12 dB (Seto et al. 2013) are the other two thresholds used in this study. The

230   minimum RR was 0.11 and 0.08 mm h^{-1} for Z_{Ka} > 12 dB and 0.16 and 0.30 mm h^{-1} for

231   Z_{Ku} > 18 dB for 2DVD and PARSIVEL^2, respectively. The sample sizes were 445 and

232   278 for Z_{Ka} > 12 dB and Z_{Ku} > 18 dB, respectively. The sample of Z_{Ka} > 12 included

233   twelve one-minute spectra that were not in the RR > 0.1 mm h^{-1} based sample.

234

235   3. Methodology

236

237   A three-parameter exponential function is employed to quantify the spatial

238   variability of the DSD. It has been widely used to determine the spatial variability of

239   rainfall through rain gauge and radar rainfall studies (Habib and Krajewski 2002,

240   Gebremichael and Krajewski 2004, Ciach and Krajewski 2006, Villarini et al. 2008,

241   Moreau et al. 2009, Tokay et al. 2014a). The Pearson correlation coefficient, r, is

242   applied to the selected DSD and rain parameters that are derived from disdrometer

243   measurements at distance d. The parametric form of exponential function is then

244   expressed as

245

246    $$r = r_0 \exp\left[(-\frac{d}{d_0})^{s_0} \right]$$ (1)

247

248   where r_0 is the correlation of a selected parameter derived from collocated

249   instruments and is known as the nugget parameter and ideally should be one.

250   However, collocated gauge and disdrometer observations show that the nugget

251 parameter ranges between 0.90 and 0.99. The other parameters of the exponential

252 function are not sensitive to changes in r_0 within this range (Schröer 2011, Tokay

253 and Özturk, 2012).   In this study, r_0 was set to 0.99. The correlation distance d_0, and

254 the shape parameter s_0, are then derived through minimizing the root mean square

255 error between the observed and derived correlations. As an initial guess, d_0 values

256 of 1 to 300 km and s_0 values of 0.1 to 2.0 were given.

257

258 The d_0 decreases with increasing s_0 when the correlation coefficient is high (Figure

259 2). When the variability is investigated over a relatively small domain as in this

260 study, the correlations of the selected DSD or rain parameters may not have a

261 decreasing trend with distance. If the correlations were high, the best fit results in

262 very high d_0 and this should not be interpreted independent of other exponential

263 function parameters. The parameters of exponential function are valid within the

264 maximum distance of the study domain (Tokay and Öztürk 2012).

265

266 4. Raindrop Size Distribution

267

268 The normalized gamma distribution function is adopted to determine the spatial

269 variability of DSD parameters. The normalization was done with respect to N_T and

270 liquid water content W (Tokay and Bashor 2010).   The normalized intercept

271 parameters with respect to total concentration, N_T^* and liquid water content, N_W are

272 expressed as

273

274 $$N_T^* = \frac{N_T}{D_{mass}}$$ (2)

275

276 $$N_w = \frac{256}{\pi \rho_w} \frac{10^3 W}{D_{mass}^4}$$ (3)

277

278 where ρ_w is the density of water. D_{mass} is related to the slope, Λ and shape

279 parameter, m of the complete gamma distribution as;

280

281 $$D_{mass} = \frac{4 + m}{\Lambda}$$ (4)

282

283 The normalized intercept parameters can then be calculated from observed spectra

284 as well. The corresponding normalized gamma fitted distributions are expressed as:

285

286 $$N(D) = N_T^* f_1(m) (\frac{D}{D_{mass}})^m \exp[-(4 + m)\frac{D}{D_{mass}}]$$ (5)

287

288 $$N(D) = N_w f_2(m) (\frac{D}{D_{mass}})^m \exp[-(4 + m)\frac{D}{D_{mass}}]$$ (6)

289

290 where $f_1(m)$ and $f_2(m)$ are given as;

291

292 $$f_1(m) = \frac{(4 + m)^{m+1}}{\Gamma(m + 1)}$$ (7)

293

294 $$f_2(m) = \frac{6}{256} \frac{(4+m)^{m+4}}{\Gamma(m+4)}$$ (8)

295

296 To extract the shape parameter, $m(N_T^*)$, and $m(N_W)$, the rain rates that are calculated

297 from observed and fitted gamma distributions (e.g. equations 5 and 6) are

298 minimized. The formulations presented above follows the complete gamma

299 function where minimum and maximum drop size is assumed zero and infinity,

300 respectively. In reality, there is a minimum and maximum drop size (D_{max}) in a

301 population of drops and the incomplete gamma function is more appropriate

302 especially if the size spectra do not contain the large drops (e.g. narrow

303 distribution), but this is the beyond the scope of this study.

304

305 The GPM DPR algorithm has adopted the normalized gamma function as in equation

306 6 (Seto et al. 2013). Since the DPR algorithm employs dual frequency reflectivity

307 measurements to determine the three parameters of gamma function, there is an

308 interest in finding relations between the derived parameters. Williams et al. (2014)

309 suggested a power law relation between the standard deviation of D_{mass} (σ_{mass}) and

310 D_{mass}. Both variables are directly calculated from observed DSD and their ratio is a

311 sole function of shape parameter, $m(\sigma_{mass})$ following complete gamma function.

312

313 $$\frac{\sigma_{mass}}{D_{mass}} = \frac{1}{(4+m)^{0.5}}$$ (9)

314

315

316   5. Probability and Cumulative Distributions

317

318   This study investigates the spatial variability of seven DSD and eight integral rain

319   parameters.   The DSD parameters include D_{mass}, D_{max}, N_T^*, N_W, $m(N_T^*)$, $m(N_W)$, and

320    $m(\sigma_{mass})$, while the rain parameters were W, RR, dual polarization parameters of

321   horizontal reflectivity (Z_H), and differential reflectivity (Z_{dr}), reflectivity at W-band

322   (Z_W), Z_{Ku}, Z_{Ka}, and dual frequency ratio (DFR = Z_{Ku}/Z_{Ka}).   The Ka-, Ku-, and W-band

323   reflectivities are calculated using Mie scattering for spherical particles, while dual-

324   polarization parameters are calculated for S-band radar following Tokay et al.

325   (2002).   Table 2 presents the mean, standard deviation, median, and 5th and 95th

326   percentage of 15 physical parameters. Both N_T^* and N_W have ranges of several order

327   of magnitude and, hence logarithmic values of these two parameters are used in

328   constructing probability and cumulative distributions.

329

330   Among many factors listed in the introduction, knowledge of the characteristics of

331   the DSD and rainfall is essential for quantifying the spatial variability.   Observed

332   DSD lacking large drops but with abundant small drops will incur different spatial

333   variability than a DSD with numerous large drops but fewer small drops.   The

334   spatial variability of rainfall, on the other hand, differs in the presence and absence

335   of heavy rain.   The probability and cumulative distributions of the DSD and rain

336   parameters provide an insight on the characteristics of DSD and rainfall, and these

337   distributions should be included if a similar study is conducted with a different

338   dataset.

339

340   Figure 3 presents the probability and cumulative distributions of fifteen DSD and

341   integral rain parameters based on 2DVD and PARSIVEL[2] measurements, when all

342   twelve units were reporting rainfall. A very good agreement in midsize range

343   (diameter 1-3 mm) of 2DVD and PARSIVEL[2] size spectra reflects an excellent

344   agreement in probability and cumulative distributions of D_{mass} between the two

345   disdrometers (Figure 2a). D_{mass} mostly resided between 0.8 and 1.5 mm, peaking at

346   1 mm (Table 2). The binning of drop counts results in quantization error in size

347   measurements in PARSIVEL[2], which is quite significant for D_{max} since the larger bins

348   have wider widths. The probability distribution of D_{max} in PARSIVEL[2] therefore had

349   multiple modes, while the probability distribution of D_{max} in 2DVD was a unimodal

350   (Figure 3b). The cumulative distributions of D_{max} agreed well between the two

351   types of disdrometers and the median D_{max} was around 1.9 mm for both (Table 2).

352

353   PARSIVEL[2] is relatively more sensitive to small drops less than 0.5 mm diameter

354   than the 2DVD (Tokay et al. 2013, 2014b). N_T^* is very sensitive to the number of

355   small drops since their concentrations are much higher than larger drops. The

356   probability distribution of $\log(N_T^*)$ of 2DVD and PARSIVEL[2] show a wide range, but

357   the PARSIVEL[2] based distribution was shifted to the larger concentrations,

358   consistent with its sensitivity to small drops (Figure 3c). N_W is more sensitive to

359   midsize drops and therefore an agreement is expected between the 2DVD and

360   PARSIVEL[2] distributions.   A general agreement is evident between the distributions

361   of log(N_W) with a median 3.55, but the PARSIVEL[2] also had low percentages of

362   log(N_w) less than 2.5 (Figure 3d).

363

364   The shape parameter of the gamma distribution is very sensitive to the method of

365   derivation and has a wide range but was mostly between 0 and 14 with mean and

366   median around 5 (Table 2). While the agreement between 2DVD and PARSIVEL[2]

367   derived distributions of shape parameters were reasonable for m(N_T^*) m(N_W), and

368   m(σ_{mass}), the probability distribution of m(N_T^*) was shifted toward larger values in

369   PARSIVEL[2] and m(N_W) and m(σ_{mass}) had slightly larger values in 2DVD (Figures 3e-

370   g).   The differences in probability and cumulative distributions are more

371   pronounced in m(N_T^*) reflecting the differences in distributions of log(N_T^*).

372

373   An excellent agreement was evident in the distributions of W, and RR between the

374   two different types of disdrometers (Figures 3h-i). Both W and RR are primarily

375   sensitive to midsize drops, while the upper end of the small drops (0.8-1.0 mm) and

376   the lower end of the large drops (3.0-4.0 mm) contribute to W and RR significantly

377   in the presence of light and heavy rainfall, respectively. The mean and median RR is

378   1.1 and 0.9 mm h^{-1}, respectively (Table 2), indicating the dominance of light rain.

379   Good agreement was also evident in distributions of Z_H, Z_{dr}, Z_W, Z_{Ku}, Z_{Ka}, and DFR

380   between the two types of disdrometers (Figures 3j-o). The median Z_H, Z_{Ku} and Z_{Ka}

381   were in the 22-23 dB range, while 95th percentiles were in the 31-32 dB range

382   (Table 2) in the presence of widespread frontal rainfall.

383

384   6. Spatial Variability

385

386   The correlations of D_{mass} and D_{max} are higher for 2DVD than for PARSIVEL[2] at a given

387   distance (Figures 4a-b). PARSIVEL[2] based correlations were 0.55-0.7 for five paired

388   observations resulting in a higher RMSE. The quantization error due to binning

389   contributed to the low correlations in PARSIVEL[2] based D_{max}. The correlations of

390   N_T^* and N_W were higher than 0.9 for all distances for the 2DVD and decreased

391   gradually with distance (Figures 4c-d). PARSIVEL[2] based correlations have a wider

392   range than 0.1 at a given distance but remained higher than 0.84 and the RMSE was

393   quite low for fitted exponential function. The correlations of shape parameters

394   decreased with distance from 0.8 to 0.5 for $m(N_T^*)$ and from 0.8 to 0.4 for $m(N_W)$

395   and $m(\sigma_{mass})$ for both 2DVD and PARSIVEL[2] (Figures 4e-g). The range of

396   correlations was less than 0.1 at a given distance for both disdrometers resulting in

397   low RMSE. The sample size was 74% and 77% of the database for $m(N_T^*)$ and

398     $m(N_W)$, respectively due to the fact that the shape parameter was outside the

399   expected range of -4 to 20 for a number of size spectrum when normalized gamma

400   function was fitted minimizing rain rate. Similarly, the sample size was 76% of the

401   database for $m(\sigma_{mass})$ due to presence of shape parameters larger than 20. The

402   large shape parameters results from narrow size spectrum in the absence of large

403   drops. The shape of size spectrum exhibits more than a single peak with a plateau

404   in midsize regime for collisional break-up dominated DSD (D'Adderio et al. 2015).

405   The gamma distribution is not the best mathematical fit in these conditions, but this

406   is beyond scope of this paper.

407

408   The correlations of RR and W decreased with distance from 0.9 to 0.55 and from

409   0.92 to 0.64, respectively (Figures 4h-i). The spread in correlation between the

410   same and different types of disdrometers was much less than 0.1 at a given distance

411   resulting in very low RMSE. Thus, the exponential fits were nearly identical for both

412   types of disdrometers. The correlations of reflectivities at different wavelengths

413   decreased with distance but there were noticeable differences and similarities

414   among them. The correlations of Z_H and Z_{Ku} were about the same at a given distance

415   for a given disdrometer while the spread in PARSIVEL[2] derived correlations of Z_{Ka}

416   were less resulting in lower RMSE (Figures 4j, 4m-n). The spread in correlations of

417   Z_W were much less (less than 0.05) at a given distance for both disdrometer types

418   resulting in an excellent fit   (Figure 4l). For Z_{dr}, there were significantly lower

419   correlations (0.35-0.55) for five PARSIVEL[2] pairs resulting in high RMSE (0.14)

420   (Figure 4k). For 2DVD, Z_{dr} decreased with distance and had a spread of 0.1 at a given

421   distance resulting in a reasonable fit with low RMSE.   DFR, which is another

422   reflectivity ratio, had lower correlations even at short distances and the spread in

423   correlations were as high as 0.3 at a given distance in PARSIVEL[2] resulting in

424   relatively poor fit with high RMSE (0.12) (Figure 4o). For 2DVD, the fit was better

425   but the spread in correlation was 0.2 at a given distance.

426

427 The correlation distances were about the same for RR and W but higher in 2DVD

428 than in PARSIVEL[2] for the rest of rain and DSD parameters (Figure 5a). For N_T^* and

429 N_W, d_0 was at around upper limit of initial guess due to high correlations for all

430 distances. The d_0 was 4.2 and 4.5 km in RR in PARSIVEL[2] and 2DVD, respectively.

431 These correlation distances correspond to high spatial variability following gauge-

432 based studies (Ciach and Krajewski 2006). However, the correlations remained

433 high (> 0.7) in this study (Figure 4i). The gauge studies were conducted for 5-

434 minute or longer integration periods while high temporal scale in this study results

435 in higher variability even in the presence of lighter rain. The shape parameter, on

436 the other hand, remained between 0.4 and 1.0 for most of the fits (Figure 5b). The

437 RMSE was less than 0.08 for almost all parameters showing the goodness of fit

438 (Figure 5c). It should be emphasized that three-parameter exponential function is

439 applied for the first time for a number of DSD and rain parameters following

440 feasibility study (Schröer 2011). Therefore, there is no direct comparison available

441 for these parameters of exponential function with any other studies.

442

443 7. Sensitivity Studies

444

445 a) Disdrometer network availability

446

447 It is not uncommon that one or more disdrometers fail to operate throughout a field

448 campaign. For spatial variability, it is important to assess the goodness of fit of the

449 three-parameter exponential function when one of the sites is not available. In that

450   regard, five out of six sites were employed to quantify the sensitivity of parameters

451   of exponential function to D_{mass} and RR. The elimination of a site reduced paired

452   correlations from 15 to 10 and if site 5 or site 6 in Table 1 were not functioning, the

453   maximum separation distance would be reduced to 1.84 km.

454

455   Fits were very good for 2DVD derived D_{mass} and RR regardless of the choice of

456   elimination of paired correlations. The d_0 had a very narrow range of 4.2-4.7 km for

457   RR but remained mostly within 11-21 km for D_{mass} (Figure 6a). For PARSIVEL[2], fits

458   were good for RR but quite poor for D_{mass} repeating previous finding in Figure 4a.

459   The d_0 had a wide range in PARSIVEL[2] derived D_{mass} but was not sensitive to the

460   elimination of any paired correlation in RR. The s_0 was less than 1.0 and highly

461   variable due to elimination of paired correlation in D_{mass} but remained mostly above

462   1.0 with almost no sensitivity to the elimination of paired correlation in RR (Figure

463   6b). The RMSE was 0.03 or less for 2DVD for both D_{mass} and RR but was higher than

464   0.1 for four trials for PARSIVEL[2] derived D_{mass} (Figure 6c).

465

466   b) Rain/No-rain threshold

467

468   The rain/no-rain threshold results in differences in the sample size and the

469   distribution of the DSD and rain parameters. The higher sensitivity DPR footprint

470   where Z_{Ka} is larger than 12 dB is expected to have less spatial variability with higher

471   d_0 than the lower sensitivity DPR footprint where Z_{Ku} is larger than 18 dB. As shown

472   in the gauge based study of Tokay and Özturk (2012), the higher thresholds

473   eliminate the light rain or low reflectivity samples and results in lower correlations,

474   especially if there is no precondition where both disdrometers must report rainfall.

475

476   Based on 2DVD observations, d_0 of D_{mass} was the lowest and the highest for Z_{Ku} and

477   RR thresholds, respectively (Figure 7a). The d_0 of RR and W was the same for RR

478   and Z_{Ka} thresholds and slightly lower for Z_{Ku} threshold. The d_0 of Z_{Ka}, Z_{Ku}, and Z_H

479   were about the same for Z_{Ka} and Z_{Ku} thresholds, and were lower than RR threshold.

480   The d_0 of DFR was the same for all three thresholds, while the other DSD and rain

481   parameters showed different trends.   The shape parameter of exponential function

482   showed little or no variability when d_0 was about the same for given thresholds

483   (Figure 7b). The RMSE did not show significant differences between the different

484   thresholds for most of the DSD and rain parameters except for Z_{dr} and DFR where

485   RMSE was noticeably higher for Z_{Ku} threshold (Figure 7c).

486

487   c) Rain coverage

488

489   Partial coverage of satellite footprint or radar pixel by rain is one of the sources of

490   NUBF and contributes significantly to the spatial variability. To quantify the spatial

491   variability in the presence of partial coverage, PARSIVEL[2] observations were

492   reprocessed when all units were reporting rainfall and when at least one unit

493   reporting rainfall. The latter is more commonly observed in nature. The sample

494   size is 4,645 one-minute size distributions for the latter condition, which makes it

495   more than 2.6 times of the sample size of the former condition. The difference is

496   mainly due to the rain intermittence. The sample size when all six PARSIVEL[2]

497   reported rainfall was 4 times larger than that when all twelve disdrometers

498   reported rainfall.

499

500   The correlation distance was distinctly lower for almost all physical parameters

501   when one or more PARSIVEL[2] reported rainfall (Figure 8a). It should also be noted

502   that d_0 was different from earlier findings when all six PARSIVEL[2] were reporting

503   rainfall. The bigger sample included more uniform rainfall across the study domain

504   and d_0 of RR was 14 km. The s_0 was higher when one or more PARSIVEL[2] reported

505   rainfall (Figure 8b). Fits were good for both conditions for physical parameters

506   except for normalized intercept and shape parameter of the gamma distribution

507   where fit was relatively poor with RMSE of 0.1 or higher (Figure 8c).

508

509   d) Rain gauge simulation

510

511   Tipping bucket rain gauges are widely used in precipitation studies but suffer from

512   significant sampling errors over short integration periods depending on the bucket

513   size (Habib et al 2001). A bucket size of 0.01 inch (0.254 mm) is used in ASOS

514   network but the gauge manufacturers also provide gauges with bucket resolutions

515   of 0.1 mm and 0.2 mm. The gauge based spatial variability of rainfall studies

516   employs 5-minute or longer integration periods to mitigate the sampling errors.

517

518   PARSIVEL^2 and 2DVD one-minute rain rate time series were employed to simulate

519   the time of tip for 0.1 mm, 0.2 mm, and 0.254 mm bucket resolutions.   The

520   simulation study ignored any disdrometer malfunctions throughout the experiment

521   period.   The 5-minute rainfall was then calculated from one-minute disdrometer

522   and three different simulated gauge datasets.   The nugget parameter of 0.99 was

523   considered in all simulations.   The correlations decrease noticeably with the size of

524   the bucket at a given distance in both PARSIVEL^2 and 2DVD based simulations

525   (Figure 9a-b).   The decrease in correlations was gradual for disdrometer but quite

526   sharp for coarser relation bucket size based simulations from nugget to short

527   separation distances.   At 2 km separation distance, the differences in correlations

528   were approximately 0.2 between disdrometer and 0.254 mm bucket simulations of

529   2DVD and PARSIVEL^2.

530

531   8. Conclusions

532

533   The pixel-scale variability of seven DSD and eight integral rain parameters was

534   investigated through a *unique* set of disdrometer observations where collocated

535   2DVD and PARSIVEL^2 were operated at six sites across the main base of NASA/WFF.

536   A three-parameter exponential function was employed to quantify the spatial

537   variability.   The r_0, or nugget parameter, was fixed to 0.99 and d_0 and s_0 were

538   retrieved minimizing RMSE following fitting an exponential function to the

539   correlations that were derived from 2DVD or PARSIVEL^2 observations.   The

540   correlations were calculated during periods when all twelve disdrometers reported

541   rainfall and a minimum RR threshold of 0.1 mm h^{-1} was satisfied with a minimum of

542   10 drops occurring in one-minute.

543

544   The there parameter exponential function is a simple mathematical form that

545   expresses the observed correlations well. It converged rapidly for almost all

546   physical parameters where RMSE was mostly less than 0.08. Very good agreement

547   between the 2DVD and PARSIVEL^2 derived correlations boosted our confidence in

548   the quality of the observations. The 2DVD outperformed the PARSIVEL^2 for

549   sampling of D_{max}, while the reverse was true for N_T^*. This is likely due to the

550   difference in the sensitivity of the respective disdrometers to the small and large

551   drop end of the size spectrum.

552

553   Given the confidence in measurement quality and fitting method, d_0 and s_0 should

554   mainly be sensitive to the characteristics of the DSD. The exclusion of a site did not

555   change the distribution of rainfall resulting in insignificant changes in d_0 and s_0 of

556   RR. The retrieved parameters of exponential function fits quite different in

557   PARSIVEL^2 derived D_{mass} when one site was removed but this is attributed to the

558   poor fitting. The d_0 and s_0 were sensitive to the different rain/no-rain thresholds.

559   They were also sensitive to the differences in conditions where one or more and all

560   six PARSIVEL^2 were reporting rainfall. The differences in the sample of

561   observations play a key role for differences in d_0 and s_0. The disdrometers have a

562   clear advantage to the rain gauges when spatial variability was studied for short

563   time intervals. The larger the bucket size the lower the correlations when the

564   disdrometer observations were used to simulate rain gauge observations at
565   different bucket size.

566

567   This is the first study where the three-parameter exponential function has been
568   used for estimating the variability of 15 physical parameters. Previously, JB12 used
569   the exponential function for RR. Their study was more robust in terms of the
570   number of available instruments and a longer period of observation.   The
571   correlations decreased more rapidly for the first 500 m reaching 0.8 in JB12 study.
572   This study did not have any paired correlation in this short distance regime and the
573   correlation of RR was about 0.9 at 500 m.   The differences in correlations are
574   attributed to the nature of rain. JB12 study included higher rainfall intensities than
575   this study.

576

577   The logistics often dominate the experiment set up and therefore the minimum and
578   maximum distances in the study domain. The sample size and type of rainfall play a
579   crucial role in quantifying the spatial variability. WFF is ideal site since rainfall from
580   multiple weather systems falls in all around year.   In this study, light rain was
581   persistent throughout field study where mean RR was 1.1 mm h^{-1} and the 95th
582   percentile of D_{max} was 3.1 mm (2DVD). For future studies, the larger domain where
583   the maximum disdrometer distance exceeds the DPR footprint and the combination
584   of light and heavy rain is desirable for quantification of spatial variability of DSD.
585   The limited but unique data set from Mid-latitude Continental Convective Clouds

586 experiment from Northern Oklahoma may prove to be a great resource for such a

587 follow-up study.

588

600

601 References

602

603 Beard, K. V., 1976: Terminal velocity and shape of cloud and precipitation drops

604 aloft. J. Atmos. Sci., 33, 851-864.

605

606 Bringi, V. N., R. Rang, and V. Chandrasekar, 2004: Evaluation of a new

607 polarimetrically based Z-R relation. J. Atmos. Oceanic. Technol., 21, 612-623.

608

609   Bringi, V., L. Tolstoy, M. Thurai, and W. Petersen, 2015: Estimation of spatial

610   correlation of rain drop size distribution parameters and rain rate using NASA's S-

611   band polarimetric radar and 2D-video disdrometer network: Two case studies from

612   MC3E. J. Hydrometeor. doi:10.1175/JHM-D-14-0204.1, in press.

613

614   Ciach, G. J., and W. F. Krajewski, 2006: Analysis and modeling of spatial correlation

615   structure of small-scale rainfall in Central Oklahoma. Adv. Water Resour., 1450-

616   1463.

617

618   D'Adderio, L. P., F. Porcu, and A. Tokay, 2015: Raindrop size distribution in the

619   presence of break-up. J. Atmos Sci. (accepted for publication).

620

621   Gebremichael, M., and W. F. Krajewski, 2004: Characterization of the temporal

622   sampling error in space-time-averaged rainfall estimates from satellite. J. Geophys.

623   Research., 109, doi: 10.1029/2004JD04509.

624

625   Habib, E., W. Krajewski, and A. Kruger, A., 2001: Sampling Errors of Tipping-Bucket

626   Rain Gauge Measurements. J. Hydrol. Eng., 6(2), 159–166.

627

628   Habib, E., and W. Krajewski, 2002: Uncertainty analysis of the TRMM ground-

629   validation radar-rainfall products: Application to the TEFLUN-B field campaign. J.

630   Appl. Meteor., 41, 558-572.

631

632   Hou, A., R. Kakar, S. Neeck, A. A. Azarbarzin, C. D. Kummerow, M. Kojima, R. Oki, K.

633   Nakamura, and T. Iguchi, 2014: The global precipitation measurement mission. Bull.

634   Amer. Meteor. Soc., 95, 701-722.

635

636   Jaffrain, J., A. Studzinski, and A. Berne, 2011: A network of disdrometers to quantify

637   the small-scale variability of the raindrop size distribution. Water Resources Resea.,

638   47, W00H06, doi:10.1029/2010WR009872.

639

640   Jaffrain, J., and A. Berne, 2012: Quantification of the small-scale spatial structure o

641   fthe raindrop size distribution from metwork of disdrometers. J. Applied Meteor.

642   Climatol., 51, 941-953.

643

644   Moreau, E., J. tested, and E. Le Bouar, 2009: Rainfall special variability observed by

645   X-band weather radar and its implication for the accuracy of rainfall estimates. Adv.

646   Water Resour., 32, 1011-1019.

647

648   Schöenhuber, M., G. Lammer, and W. L. Randeu, 2007: One decade of imaging

649   precipitation measurement by 2D video disdrometer. Adv. Geosci., 10, 85-90.

650

651   Schröer, J-B, 2011: Spatial and temporal variability of raindrop size distribution.

652   Diploma Thesis. The University of Bonn, Bonn, Germany, 133pp.

653

654   Seto, S., T. Iguchi, and T. Oki, 2013: The basic performance of a precipitation

655   retrieval algorithm for the global precipitation measurement mission's single/dual-

656   frequency radar measurements. IEEE Trans. Geoscience Rem. Sensing, 51, 5239-

657   5251.

658

659   Tapiador, F. J., R. Checa, and M. de Castro, 2010: An experiment to measure the

660   spatial variability of raindrop size distribution using sixteen laser disdrometers.

661   Geophys. Res. Lett., 37, L16803, doi: 10.1029/2010GRL044120.

662

663   Thurai, M., W. A. Petersen, A. Tokay, C. Schultz, and P. Gatlin, 2011: Drop size

664   distribution comparisons between PARSIVEL and 2-D video disdrometers. Adv.

665   Geosci., 30, 3–9.

666

667   Tokay, A., A. Kruger, W. Krajewski, P. A., Kucera, and A. J. Pereira Filho, 2002:

668   Measurements of drop size distribution in the southwestern Amazon basin. *J.*

669   *Geophys. Res.*, **107**, D20, 8052, doi:10.1029.

670

671   Tokay, A., P. G. Bashor, and K. R. Wolff, 2005: Error characteristics of rainfall

672   measurements by collocated Joss-Waldvogel disdrometers.   J. Atmos. Oceanic

673   Technol., 22, 513-527.

674

675   Tokay, A., and P. G. Bashor, 2010: An experimental study of small-scale variability of

676   raindrop size distribution. J. Hydrometeor., 11, 2348-2365.

677

678   Tokay, A., and K. Öztürk, 2012: An experimental study of the small-scale ariability of

679   rainfall. J. Hydrometeor., 13, 351-365.

680

681   Tokay, A., W. A. Petersen, P. Gatlin, and M. Wing, 2013: Comparison of raindrop size

682   distribution measurements by collocated disdrometers. J. Atmos. Oceanic Technol.,

683   30, 1672-1690.

684

685   Tokay, A., R. J. Roche, and P. G. Bashor, 2014a: An experimental study of spatial

686   variability of rainfall. J. Hydrometeor., 15, 801-812.

687

688   Tokay, A., D. B. Wolff, and W. A. Petersen, 2014b: Evaluation of the new version of

689   the laser-optical disdrometer, OTT PARSIVEL^2. J. Atmos. Oceanic Technol., 31, 1276-

690   1288.

691

692   Villarini, G., P. V. Mandapaka, W. F. Krajewski, and R. J. Moore, 2008: Rainfall and

693   sampling uncertaintites: A rain gauge perspective. J. Geophy. Resea., 113, doi:

694   10.1029/2007/JD009214.

695

696   Williams, C. R., V. N. Bringi, L. D. Carey, V. Chandrasekar, P. N. Gatlin. Z. S. Haddad, R.

697   Meneghini, S. J. Munchak, S. W. Nesbitt, W. A. Petersen, S. Tanelli, A. Tokay, A. Wilson,

698   and D. B. Wolff, 2014: Describing the shape of raindrop size distributions using

699   uncorrelated raindrop mass spectrum parameters. J. Applied Meteor. Climatol., 53,

700   1282-1296.

701

702

703

704   Figure Captions:

705

706   Figure 1. Google Map of six field sites at the NASA Wallops Flight Facility (top).

707   Picture of 2DVD, PARSIVEL[2] among other precipitation measuring instruments at

708   the Pad (middle) and at the Automated Surface Observing System site (bottom).

709   Please note that not all the instruments collecting data at the Pad during the

710   experiment period.

711

712   Figure 2. Dependence of the correlation distance to correlation coefficient at a given

713   distance and shape parameter when nugget parameter is set to 0.99. Four different

714   shape parameters and two different distances are used.

715

716   Figure 3. Probability and cumulative distributions of (a) mass weighted diameter,

717   (b) maximum diameter, (c) logarithmic normalized intercept parameter, N_T^*, (d)

718   logarithmic normalized intercept parameter, N_W, (e) shape parameter with respect

719   to N_T^*, (f) shape parameter with respect to N_W,, (g) shape parameter with respect to

720   σ_{mass}, (h) liquid water content, (i) rain rate, (j) horizontal reflectivity, (k) differential

721   reflectivity, (l) reflectivity at W-band, (m) reflectivity at Ku-band, (n) reflectivity at

722   Ka-band, (o) dual frequency ratio. Distributions of these physical parameters are

723   derived from 2DVD and PARSIVEL[2] observations.

724

725   Figure 4. Spatial variability of (a) mass weighted diameter, (b) maximum diameter,

726   (c) logarithmic normalized intercept parameter, N_T^*, (d) logarithmic normalized

727   intercept parameter, N_W, (e) shape parameter with respect to N_T^*, (f) shape

728   parameter with respect to $N_{W,}$, (g) shape parameter with respect to σ_{mass}, (h) liquid

729   water content, (i) rain rate, (j) horizontal reflectivity, (k) differential reflectivity, (l)

730   reflectivity at W-band, (m) reflectivity at Ku-band, (n) reflectivity at Ka-band, (o)

731   dual frequency ratio, all derived from 2DVD (blue dots) and PARSIVEL[2] (red stars)

732   observations.   The parameters of the three-parameter exponential function

733   including root-mean-square error and the sample size are also given.

734

735   Figure 5. (a) Correlation distance and (b) shape parameter of the three-parameter

736   exponential function and (c) root-mean-square error for fifteen physical parameters

737   based on 2DVD (blue dots) and PARSIVEL[2] (red stars) observations. Several

738   correlation distances were higher than y-axis range and are marked with their

739   values.

740

741   Figure 6. Sensitivity of (a) the correlation distance, (b) shape parameter of the

742   three-parameter exponential function and of (c) root-mean-square error of mass

743   weighted diameter (left) and rain rate (right) to the elimination of a site (e.g. site1)

744   during the experiment. Several correlation distances were higher than y-axis range

745   and are marked with their values.

746

747   Figure 7. Sensitivity of (a) the correlation distance, (b) shape parameter of the

748   three-parameter exponential function and of (c) root-mean-square error of fifteen

749   physical parameters to the rainfall threshold following 2DVD observations. The

750   rainfall thresholds of Z_{Ka} > 12 dB (green dot), Z_{Ku} > 18 dB (black dot), and RR > 0.1 m

751   h^{-1} (red dot) are considered. Several correlation distances were higher than y-axis

752   range and are marked with their values.

753

754   Figure 8. Sensitivity of (a) the correlation distance, (b) shape parameter of the

755   three-parameter exponential function and of (c) root-mean-square error of fifteen

756   physical parameters to rain coverage. One or more (orange stars) as well as all six

757   (red stars) PARSIVEL[2] reporting rainfall was considered. Several correlation

758   distances were higher than y-axis range and are marked with their values.

759

760   Figure 9. Spatial variability of 5-minute rainfall derived from (a) 2DVD and (b)

761   PARSIVEL[2] observations (red), simulated gauge at 0.1 mm bucket (blue), simulated

762   gauge at 0.2 mm bucket (green), and simulated gauge at 0.254 mm bucket (black).

763

764

765   Table 1. NASA Wallops Flight Facility Precipitation Data Acquisition Network. The

766   distances between the six sites are given in km.

767

	Site #	Site 1	Site 2	Site 3	Site 4	Site 5	Site 6
	Site name	Pad	ASOS	Balloon Launch Facility	Building A41	Visitor Center	Water Treatment Plant
	Coordinates	37.944°N, 75.464°W	37.944°N, 75.481°W	37.938°N, 75.456°W	37.934°N, 75.471°W	37.929°N, 75.473°W	37.937°N, 75.466°W
Site 1			0.51	0.60	1.25	1.34	1.41
Site 2				1.06	1.81	0.88	1.53
Site 3					1.84	1.75	1.80
Site 4						0.99	1.52
Site 5							2.31

768

769

770 Table 2: Mean, standard deviation, median, and 5th and 95th percentiles of seven

771 DSD and eight integral parameters that were derived from 2DVD and PARSIVEL[2]

772 (Par[2]) observations.

773

DSD and integral rain parameters	mean		standard deviation		median		5th percentile		95th percentile	
	2DVD	Par[2]	2DVD	Par[2]	2DVD	Par[2]	2DVD	Par[2]	2DVD	Par[2]
D_{mass} (mm)	1.11	1.09	0.30	0.32	1.05	1.01	0.72	0.72	1.64	1.63
D_{max} (mm)	2.03	1.96	0.58	0.63	1.92	1.93	1.28	1.22	3.07	3.35
N_T^* ($m^{-3}mm^{-1}$)	302	951	394	2,271	184	319	47	64	1,065	4,274
N_w ($m^{-3}mm^{-1}$)	6,524	7,313	9,294	10,915	3,468	3,588	711	53	26,787	32,706
$m(N_T^*)$	4.85	5.95	2.92	3.87	4.40	5.10	1.10	1.40	10.30	13.65
$m(N_w)$	5.16	5.00	3.38	4.01	4.50	4.00	0.80	0.10	11.40	12.90
$m(\sigma_{mass})$	5.75	5.41	3.54	4.18	5.23	4.60	0.90	-0.01	12.14	13.45
RR (mmh^{-1})	1.10	1.15	0.94	1.00	0.87	0.91	0.25	0.27	2.94	2.92
W (gm^{-3})	0.071	0.077	0.054	0.056	0.059	0.065	0.019	0.021	0.188	0.191
Z_h (dB)	26.4	27.7	18.0	33.4	22.3	22.1	15.0	15.0	31.2	31.8
Z_{dr} (dB)	0.376	0.394	0.291	0.427	0.287	0.273	0.119	0.112	0.839	0.938
Z_W (dB)	16.9	17.3	3.4	3.2	15.8	16.4	11.3	11.8	20.8	21.1
Z_{Ku} (dB)	26.8	27.7	18.5	22.1	21.9	21.7	14.8	14.7	31.7	32.7
Z_{Ka} (dB)	26.3	26.2	5.8	6.3	23.4	23.2	15.2	15.5	31.4	31.5
DFR	-0.99	-0.86	1.19	1.11	-1.27	-1.04	-2.04	-1.86	1.26	0.78

774
775
776

Figure 1. Google Map of six field sites at the NASA Wallops Flight Facility (top). Picture of 2DVD, PARSIVEL[2] among other precipitation measuring instruments at the Pad (middle) and at the Automated Surface Observing System site (bottom). Please note that not all the instruments collecting data at the Pad during the experiment period.

785
786
787
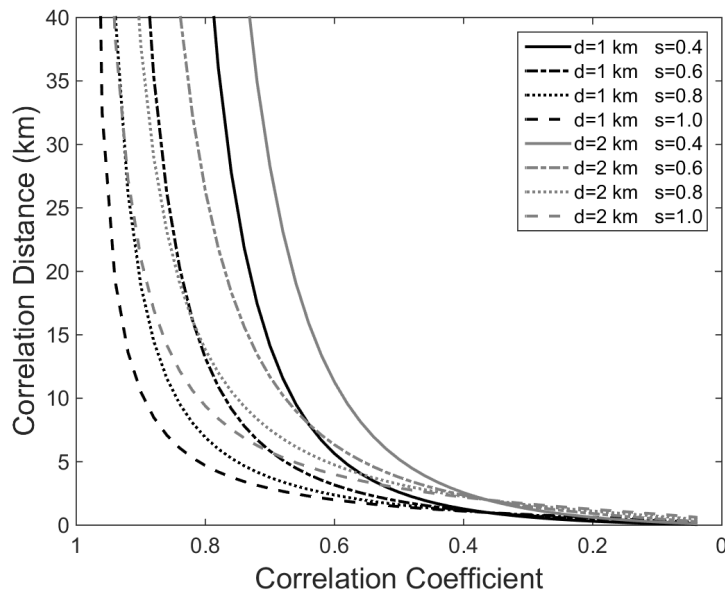788 Figure 2. Dependence of the correlation distance to correlation coefficient at a given
789 distance and shape parameter when nugget parameter is set to 0.99. Four different
790 shape parameters and two different distances are used.
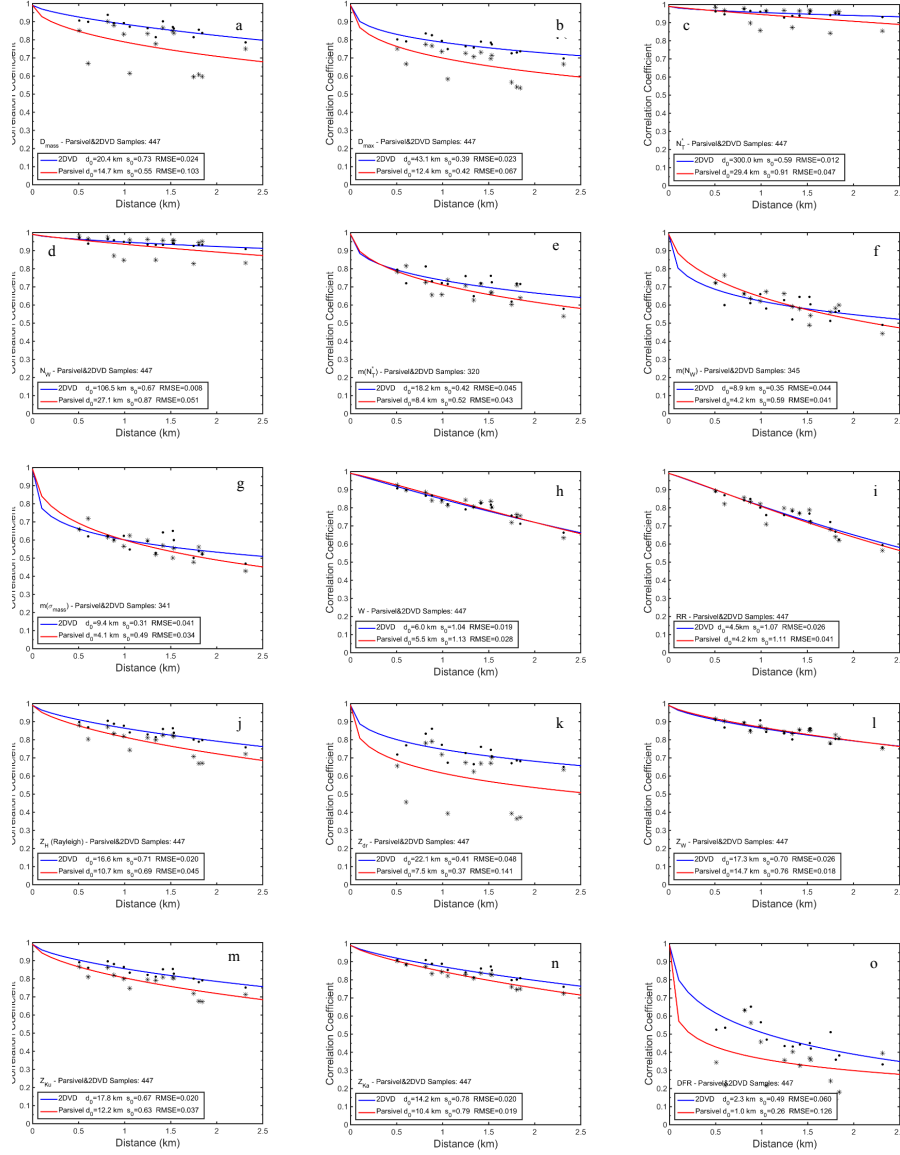791
792

794 Figure 3. Probability and cumulative distributions of (a) mass weighted diameter,
795 (b) maximum diameter, (c) logarithmic normalized intercept parameter, N_T^*, (d)
796 logarithmic normalized intercept parameter, N_W, (e) shape parameter with respect
797 to N_T^*, (f) shape parameter with respect to N_W, (g) shape parameter with respect to
798 σ_{mass}, (h) liquid water content, (i) rain rate, (j) horizontal reflectivity, (k) differential
799 reflectivity, (l) reflectivity at W-band, (m) reflectivity at Ku-band, (n) reflectivity at
800 Ka-band, (o) dual frequency ratio. Distributions of these physical parameters are
801 derived from 2DVD and PARSIVEL[2] observations.

Figure 4. Spatial variability of (a) mass weighted diameter, (b) maximum diameter, (c) logarithmic normalized intercept parameter, N_T^*, (d) logarithmic normalized intercept parameter, N_W, (e) shape parameter with respect to N_T^*, (f) shape parameter with respect to N_W, (g) shape parameter with respect to s_{mass}, (h) liquid water content, (i) rain rate, (j) horizontal reflectivity, (k) differential reflectivity, (l) reflectivity at W-band, (m) reflectivity at Ku-band, (n) reflectivity at Ka-band, (o) dual frequency ratio, all derived from 2DVD (blue dots) and PARSIVEL[2] (red stars) observations. The parameters of the three-parameter exponential function including root-mean-square error and the sample size are also given.
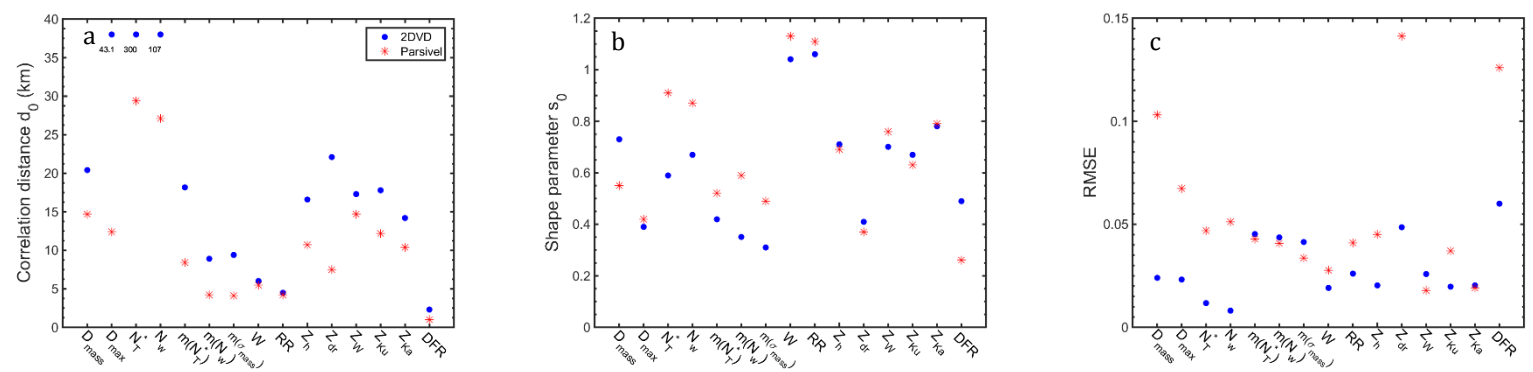
Figure 5. (a) Correlation distance and (b) shape parameter of the three-parameter exponential function and (c) root-mean-square error for fifteen physical parameters based on 2DVD (blue dots) and PARSIVEL[2] (red stars) observations. Several correlation distances were higher than y-axis range and are marked with their values.
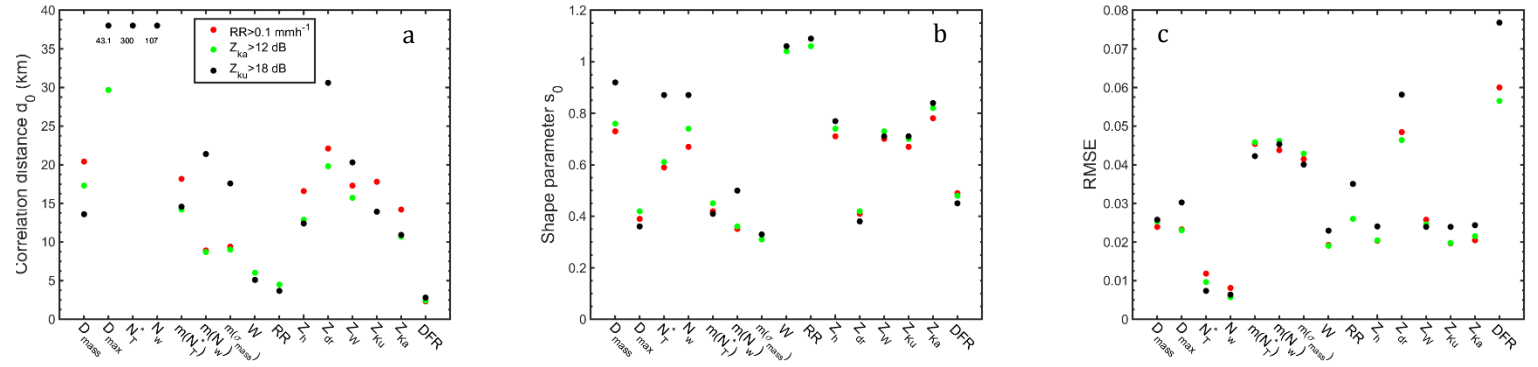
823
824
825
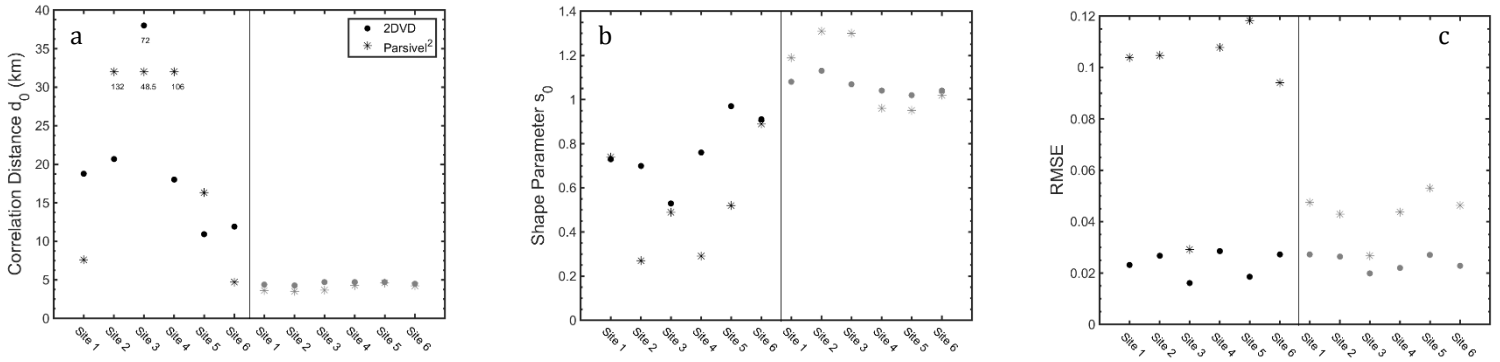
826
827 Figure 6. Sensitivity of (a) the correlation distance, (b) shape parameter of the
828 three-parameter exponential function and of (c) root-mean-square error of mass
829 weighted diameter (left) and rain rate (right) to the elimination of a site (e.g. site1)
830 during the experiment. Several correlation distances were higher than y-axis range
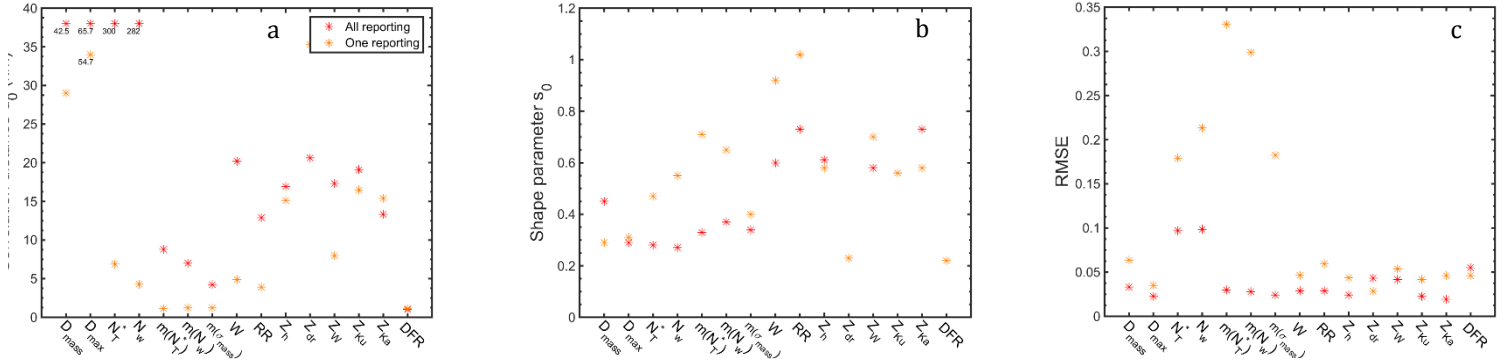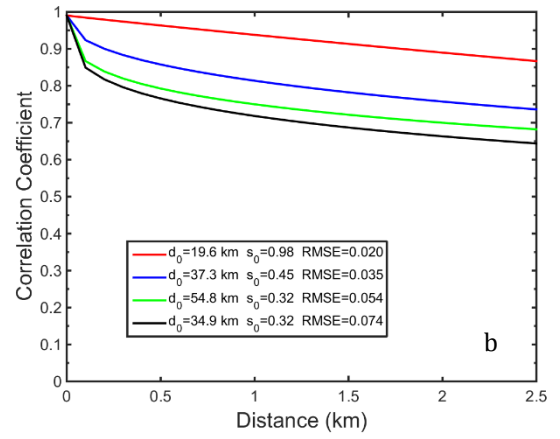831 and are marked with their values.
832
833
834
835

Figure 7. Sensitivity of (a) the correlation distance, (b) shape parameter of the three-parameter exponential function and of (c) root-mean-square error of fifteen physical parameters to the rainfall threshold following 2DVD observations. The rainfall thresholds of $Z_{Ka} > 12$ dB (green dot), $Z_{Ku} > 18$ dB (black dot), and RR > 0.1 m h^{-1} (red dot) are considered. Several correlation distances were higher than y-axis range and are marked with their values.
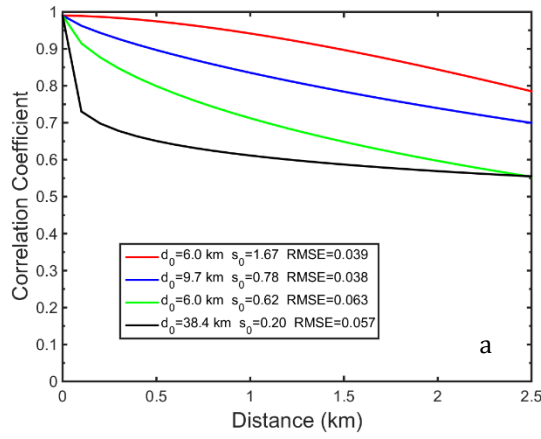
847
848 Figure 8. Sensitivity of (a) the correlation distance, (b) shape parameter of the
849 three-parameter exponential function and of (c) root-mean-square error of fifteen
850 physical parameters to rain coverage. One or more (orange stars) as well as all six
851 (red stars) PARSIVEL[2] reporting rainfall was considered. Several correlation
852 distances were higher than y-axis range and are marked with their values.
853
854
855
856

857

858
Figure 9. Spatial variability of 5-minute rainfall derived from (a) 2DVD and (b)
PARSIVEL[2] observations (red), simulated gauge at 0.1 mm bucket (blue), simulated
gauge at 0.2 mm bucket (green), and simulated gauge at 0.254 mm bucket (black).
862